AIP Journal of Applied Physics

Understanding junction breakdown in multicrystalline solar cells

Otwin Breitenstein, Jan Bauer, Karsten Bothe, Wolfram Kwapil, Dominik Lausch et al.

Citation: J. Appl. Phys. 109, 071101 (2011); doi: 10.1063/1.3562200
View online: http://dx.doi.org/10.1063/1.3562200
View Table of Contents: http://jap.aip.org/resource/1/JAPIAU/v109/i7
Published by the American Institute of Physics.

Additional information on J. Appl. Phys.

Journal Homepage: http://jap.aip.org/
Journal Information: http://jap.aip.org/about/about_the_journal
Top downloads: http://jap.aip.org/features/most_downloaded
Information for Authors: http://jap.aip.org/authors

ADVERTISEMENT

Downloaded 15 May 2013 to 134.94.122.141. This article is copyrighted as indicated in the abstract. Reuse of AIP content is subject to the terms at: http://jap.aip.org/about/rights_and_permissions

APPLIED PHYSICS REVIEWS—FOCUSED REVIEW

Understanding junction breakdown in multicrystalline solar cells

Otwin Breitenstein,[1,a)] Jan Bauer,[1,b)] Karsten Bothe,[2] Wolfram Kwapil,[3] Dominik Lausch,[4] Uwe Rau,[5] Jan Schmidt,[2] Matthias Schneemann,[5] Martin C. Schubert,[3] Jan-Martin Wagner,[1,c)] and Wilhelm Warta[3]
[1]*Max Planck Institute of Microstructure Physics, Weinberg 2, D-06120 Halle, Germany*
[2]*Institute for Solar Energy Research Hameln/Emmerthal (ISFH), Am Ohrberg 1, D-31860 Emmerthal, Germany*
[3]*Fraunhofer Institute for Solar Energy Systems (ISE), Heidenhofstraße 2, D-79110 Freiburg, Germany*
[4]*Fraunhofer Center for Silicon Photovoltaics (CSP), Walter-Hülse-Straße 1, D-06120 Halle, Germany*
[5]*IEF5-Photovoltaik, Forschungszentrum Jülich, 52425 Jülich, Germany*

(Received 29 September 2010; accepted 2 February 2011; published online 12 April 2011)

Extensive investigations on industrial multicrystalline silicon solar cells have shown that, for standard 1 Ω cm material, acid-etched texturization, and in absence of strong ohmic shunts, there are three different types of breakdown appearing in different reverse bias ranges. Between −4 and −9 V there is early breakdown (type 1), which is due to Al contamination of the surface. Between −9 and −13 V defect-induced breakdown (type 2) dominates, which is due to metal-containing precipitates lying within recombination-active grain boundaries. Beyond −13 V we may find in addition avalanche breakdown (type 3) at etch pits, which is characterized by a steep slope of the *I-V* characteristic, avalanche carrier multiplication by impact ionization, and a negative temperature coefficient of the reverse current. If instead of acid-etching alkaline-etching is used, all these breakdown classes also appear, but their onset voltage is enlarged by several volts. Also for cells made from upgraded metallurgical grade material these classes can be distinguished. However, due to the higher net doping concentration of this material, their onset voltage is considerably reduced here. © *2011 American Institute of Physics*. [doi:10.1063/1.3562200]

TABLE OF CONTENTS

I. INTRODUCTION 1
II. EXPERIMENTAL 2
III. GENERAL BREAKDOWN BEHAVIOR 2
IV. BREAKDOWN MECHANISMS 4
A. Early breakdown 4
B. Defect-induced breakdown 5
C. Avalanche breakdown 6
V. BREAKDOWN IN ALKALINE-ETCHED AND UMG CELLS 7
VI. CONCLUSIONS 8

I. INTRODUCTION

Since the electric potentials between the cells in a string of a solar module are floating, the individual cell biases strongly depend on the individual cell characteristics. If, e.g., one cell in a module should be broken or shadowed and therefore generates a considerably reduced current, this cell may become reverse-biased by the other cells in the string by −13 V and beyond. If in this cell a large reverse current flows in one site, this site may heat up excessively (generation of hot spots), which may lead to thermal destruction of the module. Therefore reverse currents in solar cells are a serious reliability issue and their origin must be well understood. The most frequent and actually trivial sources of reverse currents in solar cells are ohmic shunts. The origins of ohmic shunts are well-known. They may be caused by incomplete edge junction isolation, by cracks, by Al contamination of the emitter, or they may be material-induced.[1] In the latter case they are usually due to *n*-conducting SiC filaments crossing the bulk, which exist preferably in grain boundaries of material from the upper part of the block.[2] The present contribution will not deal with these ohmic shunts but will concentrate on junction breakdown processes under reverse bias. It will collect the most important results of several previous publications of the authors, which all have been devoted to single aspects of the general breakdown behavior, together with previously unpublished results, to form a complete overview of the present knowledge of breakdown occurring in multicrystalline silicon solar cells.

The basic research about breakdown mechanisms in crystalline silicon has ended in the late 1970s after dislocation-free Si crystals have become available. One of the latest reviews from this time is that of Mahadevan *et al*.[3] However,

a)Author to whom correspondence should be addressed. Electronic mail: breiten@mpi-halle.mpg.de.
b)Present address: CaliSolar GmbH, Magnusstraße 11, D-12489 Berlin.
c)Present address: Christian-Albrechts-Universität zu Kiel, Institut für Materialwissenschaft, Kaiserstraße 2, D-24143 Kiel.

 © 2011 American Institute of Physics

Downloaded 15 May 2013 to 134.94.122.141. This article is copyrighted as indicated in the abstract. Reuse of AIP content is subject to the terms at: http://jap.aip.org/about/rights_and_permissions

the breakdown problem has reappeared with the advent of multicrystalline silicon solar cells where light emission has been observed under reverse bias,[4] but there have been only speculations about the origin of these hot spots. The main focus so far was on avoiding thermal destruction of modules (e.g., by using bypass diodes) rather than on the investigation of the microscopic origins of the hot spots.[5,6] However, in the last years several authors have investigated the reverse *I-V* characteristic of solar cells in detail. To understand the physics behind breakdown in solar cells is one of the major issues to have an eye on in the future of silicon solar cells, and becomes even more important for the new solar cell materials like upgraded metallurgical grade (UMG) silicon.

II. EXPERIMENTAL

The results shown later in Sec. III are obtained on a few cells made industrially from adjacent wafers of standard solar-grade silicon material ($p \approx 1 \times 10^{16}$ cm^{-3}) by using standard screen-printing technology with full-area Al back contact and acidic etched texturization. In Sec. IV the physical origin of the three dominating breakdown types found in Sec. III will be dealt with by using data of the same and other but equivalent cells. In Sec. V it will be reported how the results change if alkaline etching or UMG material is used instead. All these investigations have been confirmed many times on cells from different producers, leading in all cases basically to the same results. Thus, it can be expected that the results shown here are typical for today's standard solar cell technology.

Besides dark current-voltage (*I-V*) characteristic measurements, most of the results rely on lock-in thermography[7] (LIT) under reverse bias and on electroluminescence (EL) imaging under forward[8] and reverse bias.[9,10] Under forward bias LIT allows to image low lifetime regions and any kind of shunts and under reverse bias all kinds of leakage and breakdown currents depending on the reverse bias magnitude.[7,11] LIT imaging allows one to detect all kinds of reverse currents (ohmic and junction breakdown) quantitatively. The local current density is given by the local LIT signal divided by the applied bias. The basic constraint of LIT is its limited spatial resolution, which is basically due to lateral heat diffusion. For the investigation of breakdown phenomena in solar cells, special LIT techniques have been developed for imaging different physical properties of breakdown sites quantitatively.[12] By evaluating LIT images taken in the dark (DLIT) at different temperatures and biases, images of the temperature coefficient (TC, given in % current change per K) of the local currents and of the relative slope of the local *I-V* characteristics (given in % current change per V) may be obtained. Since these parameters are normalized to the total current values, they are not influenced by the magnitude of the individual local breakdown currents but generally characterize the underlying breakdown mechanism. Finally, the presence of avalanche breakdown can be uniquely proven by quantitatively imaging the local avalanche multiplication factor (MF) of photogenerated carriers by applying a special illuminated LIT method[12] (MF-ILIT).

EL under forward bias relies on light generated by radiative recombination of electrons and holes in the bulk. The luminescence peaks at about 1100 nm and basically images the "internal voltage" in the bulk, which is strongly influenced by grown-in recombination-active crystal defects. Hence, the dark lines visible in forward-bias EL images are basically decorated grain boundaries (GBs) (random GBs, twin GBs, or small-angle GBs, which are rows of dislocations). Small-angle GBs are sometimes also called intragrain defects since they do not significantly alter the grain orientation. EL under reverse bias (called in the following ReBEL),[13] on the other hand, relies on acceleration with subsequent scattering or recombination of carriers in high electric fields. The light emission has been attributed to hot carrier interband recombination[14] or relaxation[15] and shows a wide-band spectrum including contributions in the visible range. Bremsstrahlung[16] plays obviously only a minor role.[17] The exact origin of this luminescence is still under discussion, a comparison of different models is presented, e.g., in Ref. 18. Note that this reverse bias light emission is of the same type as observed, e.g., at MOS breakdown sites or in MOSFET channel regions,[18] hence it generally appears if carriers in semiconductors are flowing under high fields. The spatial resolution of reverse-bias EL imaging is considerably better than that of LIT or forward-bias EL, since here is no blurring caused by lateral thermal or carrier diffusion. Stronger ohmic shunts locally short-circuit the *p-n* junction. Therefore they cannot be seen by reverse-bias EL imaging since there is no sufficiently high electric field in these positions.

Another technique used here for microscopic identification of avalanche breakdown sites is lock-in electron beam-induced current (EBIC) under reverse bias. While standard EBIC investigations are performed under zero bias by using dc coupling of the current amplifier, this is not possible under high reverse bias, since the breakdown current would overload the EBIC amplifier. Moreover, the breakdown current is strongly fluctuating leading to a strong noise current. Therefore for these investigations the EBIC amplifier was ac coupled to the sample,[19] the electron beam was pulsed at 1 kHz, and the signal was detected in lock-in mode.

III. GENERAL BREAKDOWN BEHAVIOR

A solar cell with a bulk doping concentration of 10^{16} cm^{-3} should show under reverse bias a saturation current in the order of 10^{-10} A/cm^2 and break down by avalanche not before -60 V.[20] In real solar cells, even in absence of ohmic shunts, the reverse characteristic at low bias is always linear (ohmic), it becomes superlinear at a few volts reverse bias, and significant breakdown may appear already at a reverse bias beyond -10 V. Figure 1 shows a typical reverse characteristic of a cell without ohmic shunts in linear drawing at two temperatures (a) and at room temperature in half-logarithmic drawing (b). We see that, at a bias beyond -13 V, the reverse current decreases with increasing temperature [negative temperature coefficient (TC), see upward arrow], and below -13 V it increases with increasing temperature (positive TC, see downward arrow). Below -13 V the characteristic is essentially exponential with a medium slope, but beyond -13 V the current steeply increases. Already this result points to the fact that obviously in different bias ranges different breakdown mechanisms dominate.

Downloaded 15 May 2013 to 134.94.122.141. This article is copyrighted as indicated in the abstract. Reuse of AIP content is subject to the terms at: http://jap.aip.org/about/rights_and_permissions

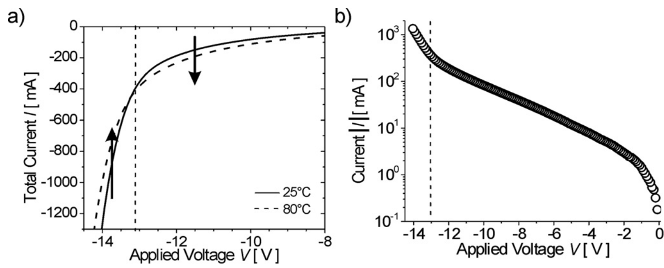

FIG. 1. Reverse current-voltage characteristic (a) in linear drawing at two temperatures and (b) at room temperature in half-logarithmic drawing (Ref. 22).

It can be expected that these different mechanisms are active in different regions of the cells. Therefore DLIT and ReBEL have been used to localize the corresponding breakdown sites. In Fig. 2, a typical cell is imaged at room temperature under three different reverse biases by DLIT (a)–(c); by ReBEL (d)−(f); and by forward-bias EL (g). All images are differently scaled to show the most important items, the scaling limits are given in the caption. The ReBEL images show a better spatial resolution than the DLIT images, as expected. The general correlation between DLIT and EL is very good, except for the images taken at −8 V. In the following, we will call all breakdown sites occurring (for our typical samples) below −9 V "early breakdown" or "type-1" breakdown sites.[21] This breakdown type is often found in edge regions and partly also in the cell area. There is no visible correlation to the forward-bias EL image (g). We have observed that some of these early breakdown sites, which are visible in DLIT, are not visible in ReBEL. The reason for this discrepancy will be discussed in Sec. IV A. Starting from −9 V more and more breakdown sites successively appear. Only between −12 and −13 V do these sites show a clear correlation to recombination-active grown-in crystal defects, see Figs. 2(b), 2(e), and 2(g). We will call this breakdown type "defect-induced" or "type-2" breakdown. The physical origin of this breakdown type will be discussed in Sec. IV B. If the reverse bias is further increased to above −13 V, a third breakdown type may become dominant, which we call "avalanche" or "type-3" breakdown. The origin of this type will be discussed in detail in Sec. IV C. It will be discussed in Sec. V that all these three different breakdown types are also present in alkaline-etched and in UMG-based solar cells, except that they exist there in different bias ranges.

The different breakdown types may exist intermixed side-by-side, so that they can hardly be separated by DLIT or even ReBEL. In favorable cases, however, in certain regions one breakdown mechanism dominates. In Fig. 2 such typical regions are indicated for the different breakdown types. It is interesting to note that not only type 1 but also type 3 is not correlated to the recombination-active crystal defects visible in Fig. 2(g). Figure 3(a) shows measured *I-V* characteristics of small pieces of solar cells which have been

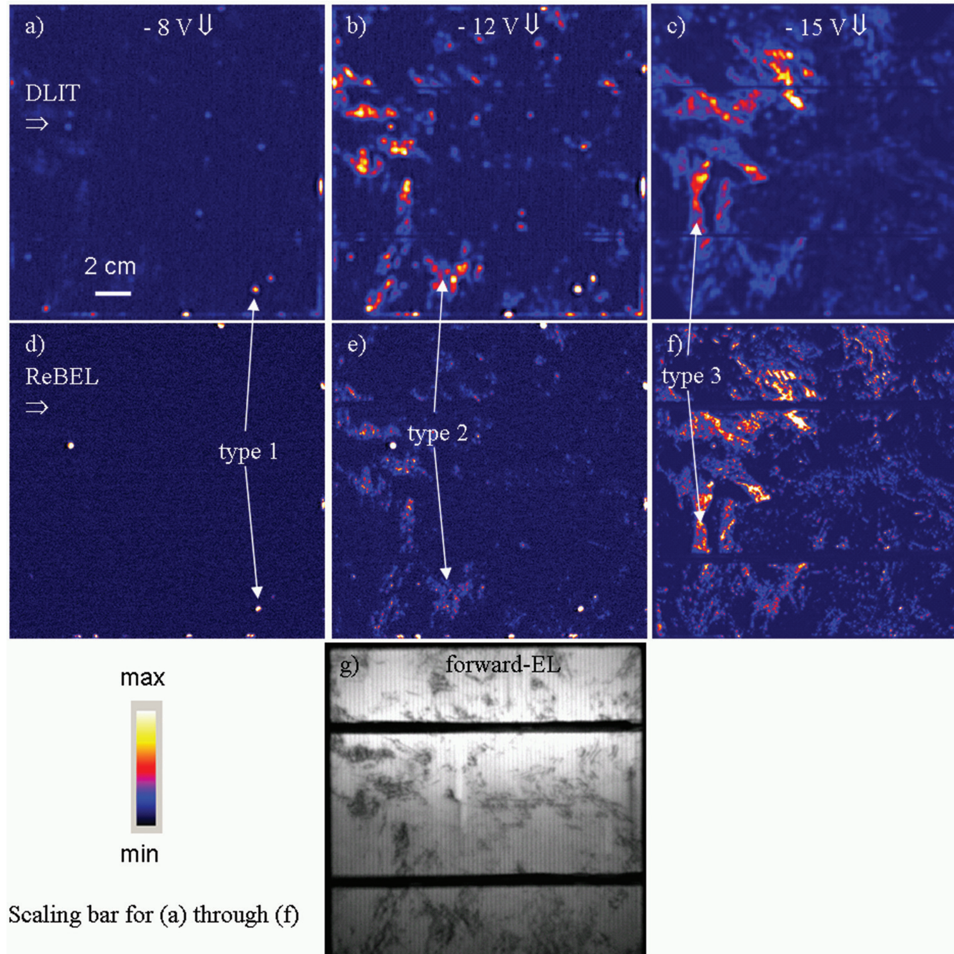

FIG. 2. (Color online) (a) DLIT at −8 V, max. 6 mK; (b) DLIT at −12 V, max. 6 mK; (c) DLIT at −15 V, max. 150 mK; (d) ReBEL at −8, 2 V, max. 100 a.u.; (e) ReBEL at −12 V, max. 100 a.u.; (f) ReBEL at −15 V, max. 1000 a.u.; (g) EL (+ 0, 6 V) 1100 a.u.

Downloaded 15 May 2013 to 134.94.122.141. This article is copyrighted as indicated in the abstract. Reuse of AIP content is subject to the terms at: http://jap.aip.org/about/rights_and_permissions

cut out so that each piece is dominated by only one breakdown type.[22] It is visible that for type 1 the current increases nearly linearly. Only beyond −13 V a steeper increase occurs, which may be due to the unintended presence of other breakdown types in this piece. For type 2 the current increases exponentially with a medium slope. For type 3 until −13 V only a weak current flows (which is probably due to other sources, e.g., the sawed edge leading to an ohmic contribution[22]), but beyond −13 V the current steeply increases. The same behavior is visible in Fig. 3(b) where data of the local ReBEL intensity (closed symbols) and of the local current density measured by DLIT (i.e., the local DLIT signal divided by the applied bias,[7] open symbols) are drawn in the positions of separately appearing breakdown types as a function of reverse bias.[23] All data sets in (b) are normalized to their value at −20 V. This figure generally confirms the results of the direct current measurement in (a). The relation between ReBEL intensity and breakdown current depends on breakdown type, but (b) proves that the ReBEL signal is at least for each breakdown type roughly proportional to the mean breakdown current density, see also Fig. 5 below. Obviously breakdown type 1 is characterized by a linear or only slightly superlinear characteristic, type 2 by an exponential one with medium slope, and type 3 by a steep current increase above a certain threshold voltage.

IV. BREAKDOWN MECHANISMS

A. Early breakdown

This breakdown type can be observed already at −5 V and below. As mentioned before, it may or may not be connected with light emission in ReBEL. It has been found recently[24] that this breakdown type is connected with Al particles at the surface, which reside on the wafer before the deposition of the silicon nitride antireflection layer and before emitter contacting. Figure 4(a) shows a microscopic ReBEL image and the corresponding topography image (b) of a particle at the surface, together with the SEM image (c) and an EDX mapping of the Al line (d) of this particle. A similar result was already shown in Ref. 1 and also[25] points

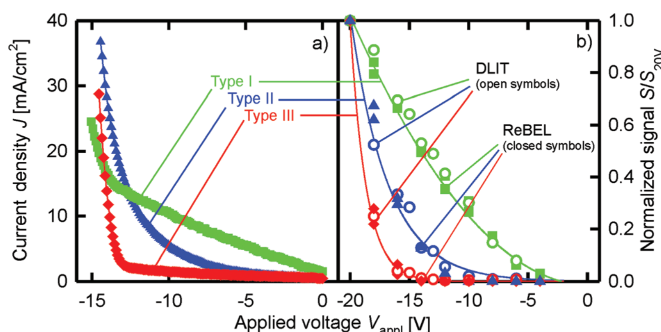

FIG. 3. (Color online) (a) Reverse *I-V* characteristics of solar cell pieces containing only one dominating breakdown type (Ref. 22). (b) ReBEL signal (closed symbols) and DLIT current density (open symbols) for several sites of each breakdown type. Reprinted with permission from K. Bothe, K. Ramspeck, D. Hinken, C. Schinke, J. Schmidt, S. Herlufsen, R. Brendel, J. Bauer, J.-M. Wagner, N. Zakharov, and O. Breitenstein, J. Appl. Phys. **106**, 104510 (2009). Copyright © 2009 American Institute of Physics.

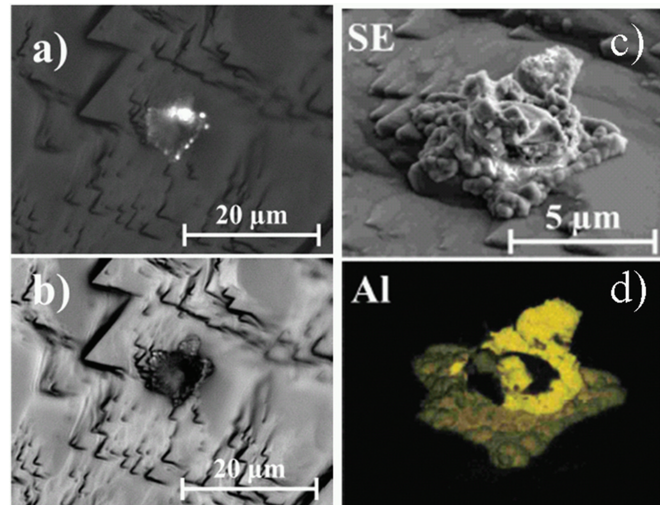

FIG. 4. (Color online) (a) Microscopic ReBEL image and (b) surface topography (reflected light image) of a particle at the surface, (c) SEM (SE) image of this particle, (d) EDX mapping of the Al line. Reprinted with permission from D. Lausch, K. Petter, R. Bakowskie, C. Czekalla, J. Lenzner, H. v. Wenckstern, and M. Grundmann, Appl. Phys. Lett. **97**, 073506 (2010). Copyright © 2010 American Institute of Physics.

to Al contamination. It is well-known that Al as a p-dopant may overcompensate the n^+-emitter if the cell is heated up, e.g., during contact firing. Then the area below an Al particle will become p^+-conducting and will be electrically in contact with the p-type base of the cell. The p^+-n^+ junction between the emitter and the Al-doped silicon yields a highly doped p-n junction. Now it depends on the size of the particle and on the amount of Al doping below the particle whether this will become a highly doped p-n junction, a weak ohmic shunt, or a strong ohmic shunt. A highly doped p-n junction may break down already at a few volts reverse bias by internal field emission (Zener effect), thereby emitting light.[26] If breakdown occurs only in microscopic spots [see light spots in Fig. 4(a)] the breakdown sites should have a high series resistance, see the following section. Therefore, for increasing reverse bias the series resistance will limit the current increase, which explains the observed linear

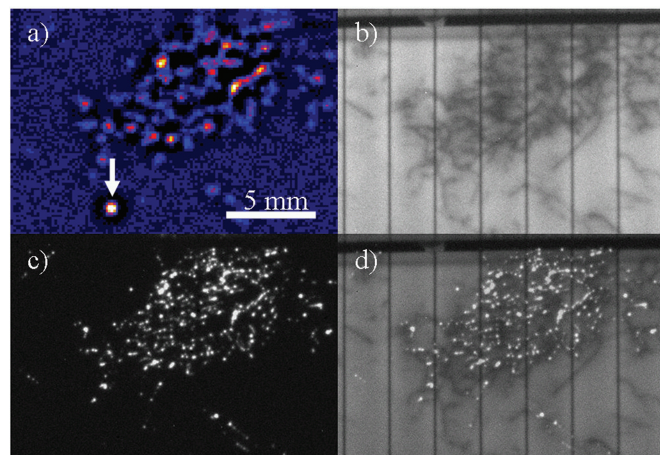

FIG. 5. (Color online) (a) High resolution DLIT image, (b) forward-bias EL image, (c) ReBEL image, and (d) superposition of (b) and (c) of a group of type-2 breakdown sites. The arrow in (a) points to an ohmic shunt.

Downloaded 15 May 2013 to 134.94.122.141. This article is copyrighted as indicated in the abstract. Reuse of AIP content is subject to the terms at: http://jap.aip.org/about/rights_and_permissions

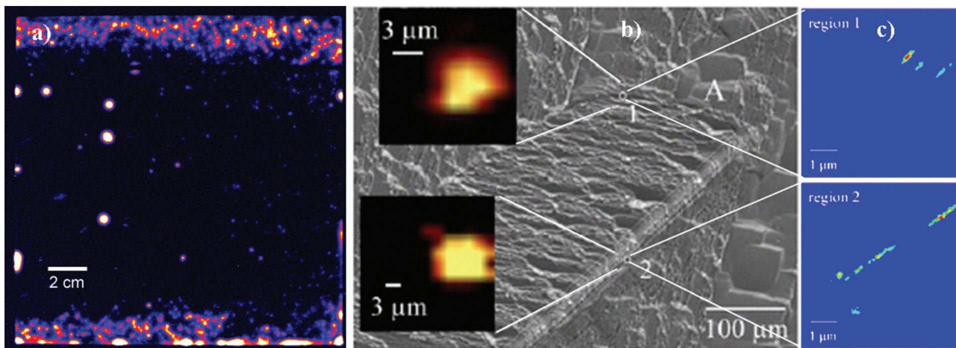

FIG. 6. (Color online) (a) DLIT image of type-2 breakdown (at −9 V), upper and lower edge region contaminated by iron, (b) SEM image of a region containing two type-2 breakdown sites (ReBEL, see insets), (c) μ-XRF mapping of iron in both breakdown sites. Reprinted with permission from W. Kwapil, P. Gundel, M. C. Schubert, F. D. Heinz, W. Warta, E. R. Weber, A. Goetzberger, and G. Martinez-Criado, Appl. Phys. Lett. **95**, 232113 (2009). Copyright © 2009 American Institute of Physics.

characteristic. If the p-doping concentration below the Al particle exceeds a certain level, the p^+-n^+ junction will become an ohmic tunnel junction. It has been discussed already at the end of Sec. II that a stronger ohmic shunt should prevent the formation of local high electric fields that are responsible for the ReBEL light emission. We believe that this is the case in those early breakdown sites which do not show ReBEL. However, if the ohmic shunt is very weak, a high field still may establish locally under reverse bias, again leading to a ReBEL signal, just as in the case of a MOSFET channel.[18]

B. Defect-induced breakdown

It was shown already in Fig. 2 that the type-2 breakdown sites correlate with recombination-active crystal defects. This correlation is demonstrated in detail in Fig. 5, showing a high-resolution DLIT image (a, 0° image at −12 V, 222 Hz lock-in frequency), a forward bias EL image (b), a ReBEL image at −12V (c), and (d) the superposition of (b) and (c) of a group of type-2 breakdown sites. It can be seen that all breakdown sites visible in DLIT are also visible in ReBEL (with one exception, see arrow), that the two signal heights are well correlating (hence the ReBEL signal is reflecting the magnitude of the breakdown current), and that all breakdown sites are lying on dark lines visible in forward bias EL (b). Similar results have been found by Usami *et al.*,[27] Wagner *et al.*,[28] and, with even better spatial resolution, by Lausch *et al.*[13] Small deviations in the position may be explained by grain boundaries lying inclined to the surface. The exception (arrow) is an ohmic shunt. This has been proven by bias-dependent DLIT investigations, it shows a linear I-V characteristic down to zero volts.

Since the dark lines in Fig. 5(b) show a constant contrast over their length, but the breakdown sites are very local, the recombination-active defect states themselves should not be responsible for the breakdown. Figure 6(a) shows a DLIT image made at −9 V of a cell made from material of a small-scale casting experiment. The upper and the lower edge were close to the edge of the crucible used. This crucible was of the same type as industrial crucibles, just being considerably smaller. It is well known that iron is the dominant impurity diffusing from the crucible walls into the edge zone of cast material.[29] Therefore, the increased breakdown site density at the top and at the bottom of Fig. 6(a) is likely due to an increased Fe contamination in these regions. Direct evidence of Fe precipitation was found recently by micro-x-ray fluorescence (μ-XRF) investigations at breakdown sites.[30] Figure 6(b) shows a SEM image of a position containing two breakdown sites in grain boundaries (see insets) together with μ-XRF mappings of iron in these two sites (c). Obviously, the type-2 breakdown originates from iron-containing precipitates lying within Fe-contaminated grain boundaries. These precipitates consist most probably of $FeSi_2$, which is metalloid. If a small $FeSi_2$ precipitate crosses the p-n junction, it yields an ohmic contact to the highly doped emitter and a Schottky contact to the base. This Schottky contact has a significantly lower equilibrium barrier height than the p-n junction and therefore breaks down earlier. Thus, this breakdown mechanism is most probably Schottky diode breakdown, which is due to field emission or thermionic field emission.[31] Figure 7 illustrates our model for type-2 breakdown. Maybe there are also other precipitate types involved in this mechanism (by TEM, besides Fe- also Cu-, Sn-, and Ca-containing precipitates have been found), and also a tip effect at the small precipitates at the base side should play a role for reducing the breakdown voltage. This explains why the onset voltage of type-2 breakdown sites spreads over an extended reverse bias range from about −9 to −13 V. Note that this breakdown type also exists on flat surfaces, where it shows somewhat higher breakdown voltages,[13] see Fig. 11.

It had been mentioned already in Sec. III that the type-2 breakdown sites are appearing with increasing reverse bias one after the other in an extended reverse bias range. The question arises whether the individual I-V characteristics of

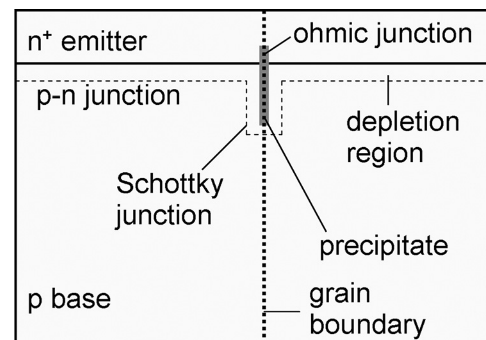

FIG. 7. Model of the precipitate-induced type-2 breakdown.

Downloaded 15 May 2013 to 134.94.122.141. This article is copyrighted as indicated in the abstract. Reuse of AIP content is subject to the terms at: http://jap.aip.org/about/rights_and_permissions

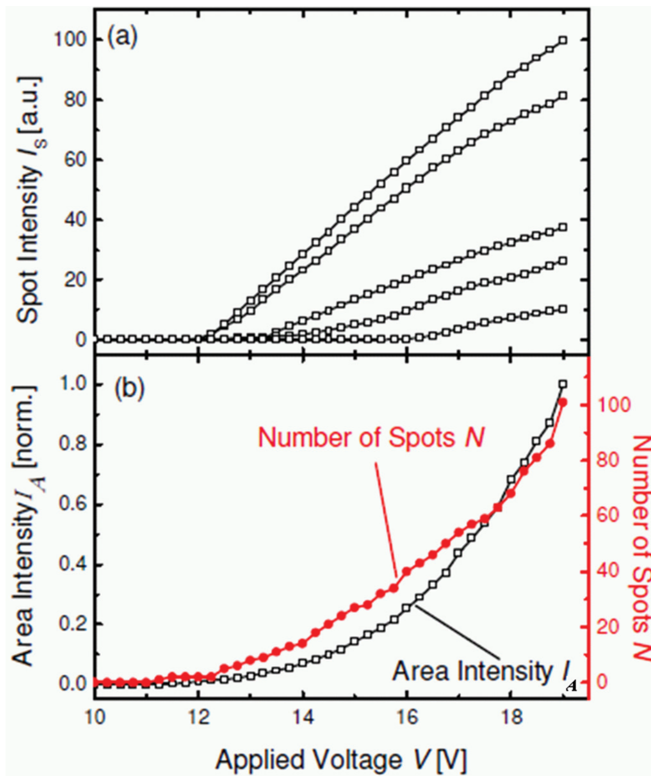

FIG. 8. (Color online) (a) ReBEL intensity of different individual type-2 breakdown sites, (b) comparison of integrated area intensity and counted number of spots in a region in an alkaline-etched cell. Reprinted with permission from M. Schneemann, A. Helbig, T. Kirchartz, R. Carius, and U. Rau, Phys. Stat. Sol. (a) **207**, 2597 (2010). Copyright © 2010 Wiley VCH.

single breakdown sites are exponential, linear, or even sublinear? In all cases the exponential *I-V* characteristic measured for these breakdown sites shown in Fig. 3 could be explained. This problem has recently been solved on alkaline-etched solar cells by applying bias-dependent high spatial resolution ReBEL investigations.[32] Note that in these cells the onset voltages are higher than in the acid-etched cells shown until now, see Ref. 13. As Fig. 8 shows, the single breakdown sites show different onset voltages and nearly linear intensity-voltage characteristics. Figure 3 and 5 have shown that the ReBEL intensity at least correlates with the breakdown current. Actually, any junction breakdown itself should show a strongly superlinear characteristic. However, since these breakdown sites are of submicron size, they are coupled to the terminals of the cell by a relatively high series resistance, which linearizes the individual characteristics. The even slightly sublinear type of the intensity-voltage characteristics can probably be explained by the increasing sample temperature with increasing reverse bias, which may lead to a reduced optical quantum efficiency or an increased series resistance. Obviously the exponential *I-V* characteristic results mainly from the appearance of new breakdown sites, as Fig. 8(b) shows. Interestingly, the intensity-voltage characteristics of the breakdown sites with a higher onset voltage show a lower slope, which is not understood yet. If a larger number of breakdown sites of the same type is evaluated, the results scatter much more, but this dependence remains still visible.[33]

Under the coarse assumption that a single breakdown region has a diameter of 1 μm, the series resistance to it both in the emitter and in the base can be estimated. Here we assume that the current spreading occurs radially half-bowl-shaped in the bulk and circle-shaped in the emitter. Moreover we assume that this geometry remains in the bulk up to the bulk thickness (0.2 mm) and in the emitter up to a distance of 1 mm, corresponding to a defect position between two grid lines. It turns out that the result only weakly depends on the upper integration boundaries, hence the deviation of the current spreading geometry from a bowl or circle one is not important. For typical values of the base resistivity of $\rho = 1\ \Omega$ cm and the emitter sheet resistance of $\rho_s = 50\ \Omega^{sqr}$ we obtain

$$R_b = \rho \int_{0.5\,\mu m}^{0.2\,mm} \frac{1}{2\pi r^2} dr = 3.2 k\Omega,\ R_e = \rho_s \int_{0.5\,\mu m}^{1\,mm} \frac{1}{2\pi r} dr = 60\Omega. \quad (1)$$

C. Avalanche breakdown

The acidic etching solution, which is used today for isotropic texturization of multicrystalline solar cells, actually is optimized not to lead to etch pits at crystal defects like dislocations. Nevertheless, in some regions etch pits may exist. It has been found that these etch pits are leading to avalanche-type breakdown.[34] This breakdown type is characterized by a steep (thresholdlike) *I-V* characteristic and a negative temperature coefficient (TC) of the current, since the mean scattering energy of carriers in the field reduces with increasing temperature. Moreover, multiplication of light-induced carriers occurs only under avalanche conditions, which may be used as a proof of avalanche breakdown occurring. Figure 9 shows images of the avalanche multiplication factor MF (a), of the TC (b), and of the slope (c), all measured at −15 V on the cell used for Fig. 2 by using special LIT methods.[12] In

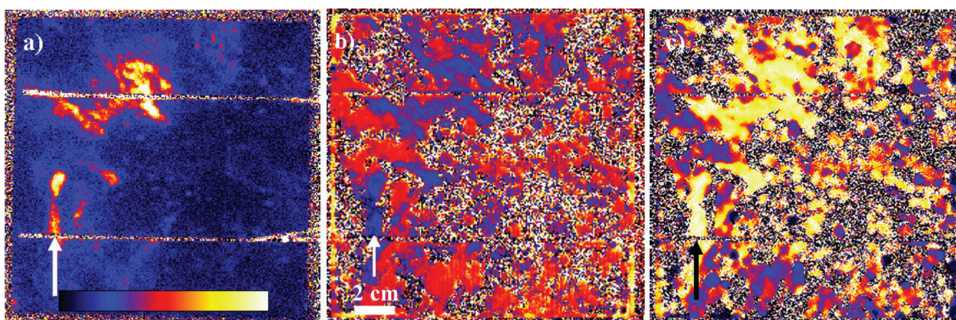

FIG. 9. (Color online) (a) Avalanche multiplication factor (0 to 3), (b) temperature coefficient (−3 to +3%/K), and (c) relative slope of the current (0 to 200%/V) of the cell used for Fig. 2, all measured at −15 V at room temperature. The arrows point to a position where pure avalanche breakdown occurs.

Downloaded 15 May 2013 to 134.94.122.141. This article is copyrighted as indicated in the abstract. Reuse of AIP content is subject to the terms at: http://jap.aip.org/about/rights_and_permissions

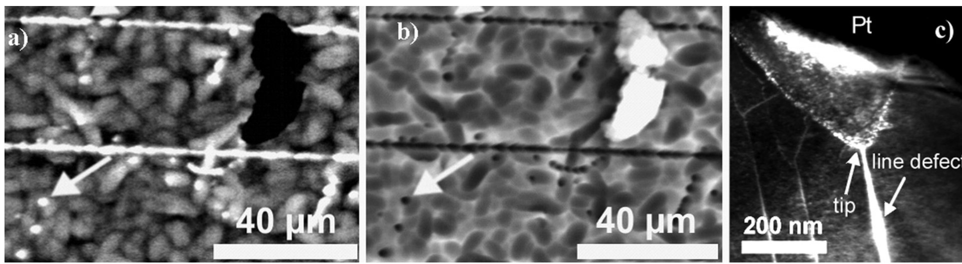

FIG. 10. (a) Lock-in EBIC image at −15 V showing microplasma (arrow) in a type-3 breakdown site, (b) SE image, (c) TEM cross section image of the tip of an etch pit. Reprinted with permission from J. Bauer, J.-M. Wagner, A. Lotnyk, H. Blumtritt, B. Lim, J. Schmidt, and O. Breitenstein, Phys. Stat. Sol. RRL 3, **40** (2009). Copyright © 2009 Wiley VCH.

the position indicated by the arrows there is considerable avalanche carrier multiplication, a clearly negative TC and a high slope of the breakdown current. At −12 V, in this position was no breakdown visible yet in Figs. 2(b) and 2(e), and in Fig. 2(g) there are no recombination-active crystal defects.

By using lock-in EBIC under −15 V reverse bias, microscopic carrier multiplication sites (microplasma) could be found in the positions of etch pits, e.g., that indicated by the arrows in Fig. 10.[34] The cross-sectional TEM image (c) shows that the tip radius is in the order of 20 nm. Since the *p-n* junction is expected to lie 300 nm below the surface, at the tip of the etch pit it should be bowl-shaped with a radius of 300 nm. Sze and Gibbons[20] have shown that under this condition the breakdown voltage for 10^{16} cm^{-3} material reduces from −60 to −13 V, which is exactly the avalanche threshold measured by us. Thus, at least for acid-etched cells, the hard breakdown type 3 appearing beyond −13 V is due to avalanche occurring at etch pits. The same threshold has been found also in alkaline-etched cells,[33] where obviously also sharp kinks in the shape of the *p-n* junction plane exist. Since also these breakdown sites are microscopic, their individual characteristics should also be linearized by a high series resistance as shown for type-2 sites in Fig. 6(a). However, in contrast to the type-2 sites, all type-3 sites show nearly the same breakdown voltage, since for all of them the geometry and the doping concentration are the same. Indeed, this has been confirmed recently by bias-dependent local ReBEL investigations.[33] Therefore, close to the onset voltage, the averaged slope of the breakdown current in type-3 breakdown sites is much higher than for sites with type-2 breakdown. Note also the considerably higher local density of type-3 sites (see Fig. 10) compared to type-2 sites (see Fig. 5). This is the reason for the kink in the global reverse characteristic at −13 V shown in Fig. 1(b).

The question arises where these etch pits come from. They are certainly not due to simple dislocations, since the dislocation density in this material is much higher than the etch pit density, and also in Fig. 10(c) some more dislocations are visible which do not lead to etch pits. Recent TEM investigations on such an etch pit have shown that the corresponding line defect is lying in a 10 nm wide 180° twin lamella extended in $[1\ 1\ \bar{1}]$-orientation.[35] This is the reason why these etch pits are often lying in rows. The line defects are dislocations in $[1\ \bar{1}\ 0]$ direction embedded in one of the twin boundaries, which are split by about 3 nm and seem to be heavily decorated at one side, probably by carbon. The origin of these defects and the reason why they lead to etch pits is not clear yet.

V. BREAKDOWN IN ALKALINE-ETCHED AND UMG CELLS

Systematic investigations have shown that at least type-1 and type-2 breakdown exists also in alkaline-etched cells, except that there, for a given net doping concentration, the threshold voltages are about 2–4 volts higher. This was nicely shown for type-2 breakdown sites by Lausch *et al.*,[13] see Fig. 11. The difference in the breakdown voltages can

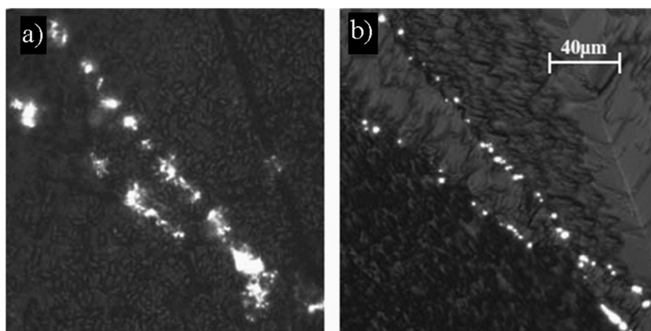

FIG. 11. ReBEL images of type-2 breakdown in cells made from adjacent wafers, (a) at −13 V on an acid-etched and (b) at −17 V on an alkaline-etched cell. Reprinted with permission from D. Lausch, K. Petter, H. v. Wenckstern, and M. Grundmann, Phys. Stat. Sol. RRL 3, **70** (2009). Copyright © 2009 Wiley VCH.

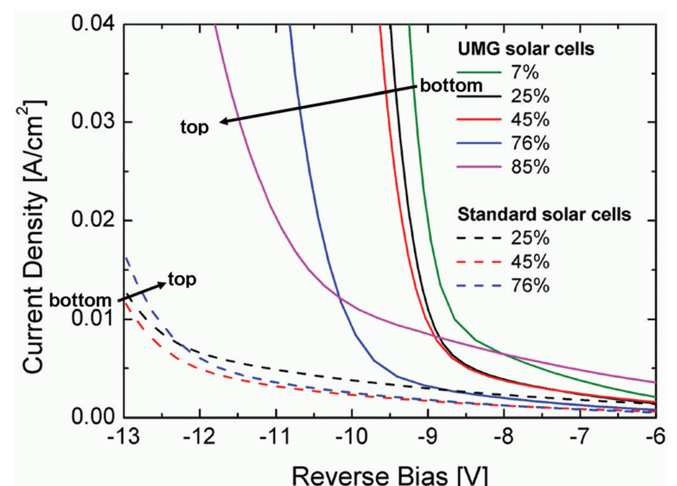

FIG. 12. (Color online) Reverse characteristics of cells from different ingot heights (given in %) of standard material (dashed lines) and UMG material (full lines).

Downloaded 15 May 2013 to 134.94.122.141. This article is copyrighted as indicated in the abstract. Reuse of AIP content is subject to the terms at: http://jap.aip.org/about/rights_and_permissions

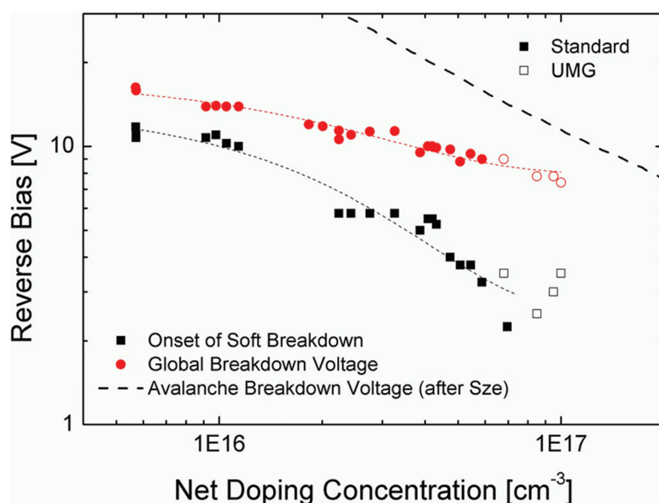

FIG. 13. (Color online) Different representations of the diode breakdown voltage versus the net doping concentration in the base of standard and UMG solar cells. The circles depict the voltage of maximum curvature in the global reverse characteristics while the rectangles show the approximate reverse voltage at which first breakdown ReBEL emission is detected at soft breakdown sites (thin dashed lines serve as guides to the eye). For comparison, the thick dashed line represents the expected avalanche breakdown voltage for defect-free one-sided abrupt *p-n* junctions (Ref. 20). Reprinted with permission from W. Kwapil, M. Wagner, M. C. Schubert, and W. Warta, J. Appl. Phys. **108**, 023708 (2010). Copyright © 2010 American Institute of Physics.

probably be related to the higher roughness of acid-etched surfaces, which leads to higher field strengths. The investigation of avalanche effects in alkaline-etched cells is still underway. Though there are no etch pits in alkaline-etched cells, the results shown in Ref. 33 indicate that there are also sites showing a clear threshold at −13 V, which should be type 3.

It had been suspected in the past that UMG material should be heavily polluted by metallic impurities. However, it has turned out that metals are no serious efficiency-limiting factor in UMG cells. Obviously the metal concentration in this material is low enough that the standard cell process, which may tolerate a relatively high metal contamination, is not negatively affected yet. However, it can be expected that residual metal contamination influences the breakdown behavior of UMG cells. Another problem of UMG material is the high residual B and P concentration, which leads to a high net doping concentration in the lower part of the ingot and decreasing net doping concentration toward the top, where the conductivity changes to *n*-type.[36] It is well known that the net doping concentration strongly influences the breakdown behavior.[37] Figure 6(a) also proves that Fe contamination increases the type-2 breakdown current. The question now is: Which of the two factors (metal contamination or net doping concentration) dominates the breakdown behavior of UMG cells? This can be checked, e.g., by comparing the breakdown currents of cells from different heights in a UMG block. From bottom to top the metal concentration should increase due to the low segregation coefficient of all metals, but the net doping concentration decreases since P has a lower segregation coefficient than B. Hence, if the breakdown current increases toward the top, the influence of the metal contamination dominates, and if it decreases the net doping concentration influence dominates. Figure 12 shows that for standard material the influence of contamination is dominating, but for UMG material the influence of the net doping concentration dominates. Note that for this judgment the current contribution which is strongly increasing toward high reverse bias is decisive, since the slowly rising current at low reverse bias is governed by ohmic shunts.

In a thorough analysis recently published by Kwapil *et al.*,[38] breakdown voltages of cells made from standard and UMG material with various net doping concentrations were measured and compared by two different criteria, see Fig. 13. In this graph the UMG cells (open symbols) smoothly fit to the standard cells (full symbols), which proves that the high net doping concentration is the main reason for early breakdown in UMG material.

VI. CONCLUSIONS

It has been demonstrated here that there are three clearly distinguishable breakdown mechanisms in multicrystalline solar cells: Early breakdown caused by Al contamination (type 1), defect-induced breakdown caused by $FeSi_2$ or other precipitates lying in grain boundaries (type 2), and avalanche breakdown caused by etch pits or other sharp kinks in the *p-n* junction plane (type 3). The question is which type of breakdown is most dangerous? Note that the investigations shown here have been made on cells without strong ohmic shunts. The type-1 "breakdown" sites are at best weak ohmic shunts, so they are not harmful at all since their current increases only linearly with reverse bias. Nevertheless, Al contamination at the surface has to be avoided, since heavy Al contamination leads to strong ohmic shunts, which also may lead to hot spots under reverse bias. Ohmic hot spots may also be caused by incomplete edge junction isolation, by cracks, or by grown-in SiC filaments.[1] The defect-induced breakdown type 2 is often the dominating one in the interesting bias range up to −13 V. However, as Figs. 2(b) and 2(e) show, there are usually many of these breakdown sites distributed across the cell area. As Fig. 8 shows, the individual breakdown currents are series resistance limited, high breakdown currents only establish by a large number of breakdown sites. Hence, even if the type-2 breakdown current is large, it should not easily lead to dangerous hot spots, since the heat distributes across the whole cell area and the local density of the breakdown sites is low. This is not the case anymore for type-3 (avalanche) breakdown. Though also these individual breakdown sites are series resistance-limited, we have observed that they may cover only a small fraction of the area with a high local density of breakdown sites, and beyond a certain reverse bias the avalanche breakdown current dominates. Thus, if the net doping concentration is high enough that significant avalanche breakdown occurs in the interesting bias range up to −13 V (e.g., UMG material), this breakdown type may become as dangerous as are strong ohmic shunts. Therefore it should be interesting to further investigate the generation of these special etch pits in acid-etched cells and maybe to avoid their formation.

These investigations do not answer the question yet why the total breakdown current of the whole cell flowing at

Downloaded 15 May 2013 to 134.94.122.141. This article is copyrighted as indicated in the abstract. Reuse of AIP content is subject to the terms at: http://jap.aip.org/about/rights_and_permissions

weak reverse bias shows a clearly positive temperature coefficient (TC), see Fig. 1(a). Note that both the early breakdown (type 1) and the defect-induced breakdown (type 2) show a negative or close to zero TC in TC-DLIT images.[12,22] However, in addition to breakdown types 1, 2, and 3, there are other current contributions which have not been discussed yet. One is the edge current, which flows at the edge of the cells where the *p-n* junction plane reaches the surface. Just as the reverse current caused by scratches, this current is probably due to hopping conduction across closely coupled gap states at the surface.[39] The edge current clearly has a positive temperature coefficient, which also has been proven by TC-DLIT,[12,22] see also Fig. 9(b). Another contribution is an obviously more or less homogeneous reverse current contribution, which has recently been observed in multicrystalline cells by T-dependent DLIT imaging.[22,28] This contribution needs very long data acquisition times to be imaged by TC-DLIT since its DLIT signal is very low. In Fig. 9(b) it is still embedded in noise or dominated by the other signals. However, since it flows homogeneously, it may contribute significantly to the total current. Also this current has a clearly positive TC.[22,28] The physical origin of this current contribution is not clear yet. Since it does not saturate like the reverse current of an ideal diode but instead depends linearly on the reverse bias and does not fit to the parameters of the forward *I-V* characteristic, it can be excluded that this is one of the two saturation current densities J_{01} or J_{02} in the normal two-diode model. The latter two current contributions also should not be homogeneously distributed, as found for the new reverse current contribution in Refs. 22 and 28 but very inhomogeneous as found by all previous DLIT experiments under forward bias on multicrystalline cells.

Of course, this review can only summarize the state of knowledge about this topic at a certain time, which is about May 2010 in this case. A number of questions still need to be answered. For example, there is no TEM confirmation yet of the defects being responsible for the type-2 breakdown, and the line defect being responsible for type-3 breakdown in acid-etched material has been identified by TEM only once.[35] Moreover, the sites showing avalanche breakdown in alkaline-etched cells have not been identified yet, and the origin of the newly found homogeneous reverse current contribution in multicrystalline cells is still unclear. Also the temperature behavior of all breakdown types still has to be investigated systematically. Thus, the research in this field is still ongoing.

ACKNOWLEDGMENTS

This work was supported by the BMU Project No. 0 327 650 "SolarFocus." The authors are grateful to H. Blumtritt, N. Zakharov, U. Hlawatsch (all Halle), and A. Lotnyk (Kiel) for experimental cooperation and to T. Kirchartz (Jülich) for discussing the text. WILEY-VCH (Weinheim) is acknowledged for their permission to reproduce Figs. 8–11.

[1]O. Breitenstein, J. P. Rakotoniaina, M. H. Al Rifai, and M. Werner, Prog. Photovoltaics **12**, 529 (2004).
[2]J. Bauer, O. Breitenstein, and J.P. Rakotoniaina, Phys. Status Solidi A **204**, 2190 (2007).
[3]S. Mahadevan, S.M. Hardas, and G. Suryan, Phys. Status Solidi A **8**, 335 (1971).
[4]Y. Kaji, H. Kondo, Y. Takahashi, T. Yamazaki, Y. Uraoka, and T. Fuyuki, *Proceedings of the 31st IEEE Photovoltaic Specialists Conference*, Orlando (IEEE, Piscataway, NJ, 2005), pp. 1346–1348.
[5]*Handbook of Photovoltaic Science and Engineering*, edited by A. Luque and S. Hegedus (Wiley, New York, 2003), pp. 297–299.
[6]M.C. Alonso-García, J.M. Ruiz, and F. Chenlo, Sol. Energy Mater. Sol. Cells **90**, 329 (2006).
[7]O. Breitenstein, W. Warta, and M. Langenkamp, *Lock-in Thermography - Basics and Use for Evaluating Electronic Devices and Materials*, 2nd ed. (Springer, Berlin, 2010).
[8]T. Fuyuki, H. Kondo, T. Yamazaki, Y. Takahashi, and Y. Uraoka, Appl. Phys. Lett. **86**, 262108 (2005).
[9]R. Newman, Phys. Rev. **100**, 700 (1955).
[10]M. Kasemann, W. Kwapil, M. C. Schubert, H. Habenicht, B. Walter, M. The, S. Kontermann, S. Rein, O. Breitenstein, J. Bauer, A. Lotnyk, B. Michl, H. Nagel, A. Schütt, J. Carstensen, H. Föll, T. Trupke, Y. Augarten, H. Kampwerth, R. A. Bardos, S. Pingel, J. Berghold, W. Warta, and S. W. Glunz, *Proceedings of the 33rd IEEE Photovoltaic Specialists Conference*, San Diego (IEEE, Piscataway, NJ, 2008), paper No. 148.
[11]J.-M. Wagner, J. Bauer, A. Lotnyk, and O. Breitenstein, *Proceedings of the 23rd European Photovoltaic Solar Energy Conference and Exhibition*, Valencia, Spain (WIP, Munich, 2008), pp. 1164–1168.
[12]O. Breitenstein, J. Bauer, J.-M. Wagner, and A. Lotnyk, Prog. Photovoltaics **16**, 679 (2008).
[13]D. Lausch, K. Petter, H. v. Wenckstern, and M. Grundmann, Phys. Status Solidi (RRL) **3**, 70 (2009).
[14]A. G. Chynoweth and K. G. McKay, Phys. Rev. **102**, 369 (1956).
[15]W. Haecker, Phys. Status Solidi A **25**, 301 (1974).
[16]T. Figielskiand and A. Torun, in *Proceedings of the 6th International Conference on the Physics of Semiconductors* (Pergamon, London, 1962), pp. 863–868.
[17]A. L. Lacaita, F. Zappa, S. Bigliardi, and M. Manfredi, IEEE Trans. Electron. Devices **40**, 577 (1993).
[18]J. Bude, N. Sano, and A. Yoshii, Phys. Rev. B **45**, 5848 (1992).
[19]O. Breitenstein, J. Bauer, M. Kittler, T. Arguirov, and W. Seifert, Scanning **30**, 331 (2008).
[20]S. M. Sze and G. Gibbons, Solid-State Electron. **9**, 831 (1966).
[21]W. Kwapil, M. Kasemann, P. Gundel, M.C. Schubert, W. Warta, P. Bronsveld, and G. Coletti, J. Appl. Phys. **106**, 063530 (2009).
[22]J. Bauer, Ph.D. thesis, Martin Luther University Halle–Wittenberg, 2009, http://digital.bibliothek.uni-halle.de/hs/urn/urn:nbn:de:gbv:3:4-1951
[23]K. Bothe, K. Ramspeck, D. Hinken, C. Schinke, J. Schmidt, S. Herlufsen, R. Brendel, J. Bauer, J.-M. Wagner, N. Zakharov, and O. Breitenstein, J. Appl. Phys. **106**, 104510 (2009).
[24]D. Lausch, K. Petter, R. Bakowskie, C. Czekalla, J. Lenzner, H. v. Wenckstern, and M. Grundmann, Appl. Phys. Lett. **97**, 073506 (2010).
[25]J. W. Bishop, Solar Cells **26**, 335 (1989).
[26]A. G. Chynoweth and K. G. McKay, Phys. Rev. **106**, 418 (1957).
[27]N. Usami, K. Kutsukake, K. Fujiwara, I. Yonenaga, and K. Nakajima, Appl. Phys. Express **1**, 075001 (2008).
[28]J.-M. Wagner, J. Bauer, and O. Breitenstein, *Proceedings of the 24th European Photovoltaic Solar Energy Conference*, Hamburg, Germany (WIP, Munich, 2009), pp. 925–929.
[29]T. Uberg Nærland, L. Arnberg, and A. Holt, Prog. Photovoltaics **17**, 289 (2009).
[30]W. Kwapil, P. Gundel, M. C. Schubert, F. D. Heinz, W. Warta, E. R. Weber, A. Goetzberger, and G. Martinez-Criado, Appl. Phys. Lett. **95**, 232113 (2009).
[31]E. H. Rhoderick and R. H. Williams, *Metal-Semiconductor Contacts* (Clarendon, Oxford, 1988).
[32]M. Schneemann, A. Helbig, T. Kirchartz, R. Carius, and U. Rau, Phys. Status Solidi A **207**, 2597 (2010).
[33]M. Schneemann, T. Kirchartz, R. Carius, U. Rau, and A. Helbig, *Proceedings of the 25th European Photovoltaic Solar Energy Conference and Exhibition*, Valencia, Spain (WIP, Munich, 2010), pp. 24–28.
[34]J. Bauer, J.-M. Wagner, A. Lotnyk, H. Blumtritt, B. Lim, J. Schmidt, and O. Breitenstein, Phys. Status Solidi (RRL) **3**, 40 (2009).
[35]O. Breitenstein, J. Bauer, J.-M. Wagner, N. Zakharov, H. Blumtritt, A. Lotnyk, M. Kasemann, W. Kwapil, and W. Warta, IEEE Trans. Electron Devices **57**, 2227 (2010).

Downloaded 15 May 2013 to 134.94.122.141. This article is copyrighted as indicated in the abstract. Reuse of AIP content is subject to the terms at: http://jap.aip.org/about/rights_and_permissions

[36]C. Modanese, M. Di Sabatino, A.-K. Søiland, K. Peter, and L. Arnberg, Prog. Photovoltaics **19**, 45 (2011).
[37]M. Wagner, B. Gründig-Wendrock, P. Palinginis, and C. Knopf, *Proceedings of the 24th European Photovoltaic Solar Energy Conference and Exhibition*, Hamburg (WIP, Munich, 2009), pp. 2028–2031.
[38]W. Kwapil, M. Wagner, M. C. Schubert, and W. Warta, J. Appl. Phys. **108**, 023708 (2010).
[39]O. Breitenstein, P. Altermatt, K. Ramspeck, and A. Schenk, *Proceedings of the 21st European Photovoltaics Energy Conference, Dresden, Germany* (WIP, Munich, 2006), pp. 625–628.

Downloaded 15 May 2013 to 134.94.122.141. This article is copyrighted as indicated in the abstract. Reuse of AIP content is subject to the terms at: http://jap.aip.org/about/rights_and_permissions